国外大学优秀教材——材料科学与工程系列（影印版）

Buddy D. Ratner, Allan S. Hoffman, Frederick J. Schoen
Jack E. Lemons

生物材料科学
医用材料导论（第2版）
Biomaterials Science:
An Introduction to Materials in Medicine
(Second Edition)

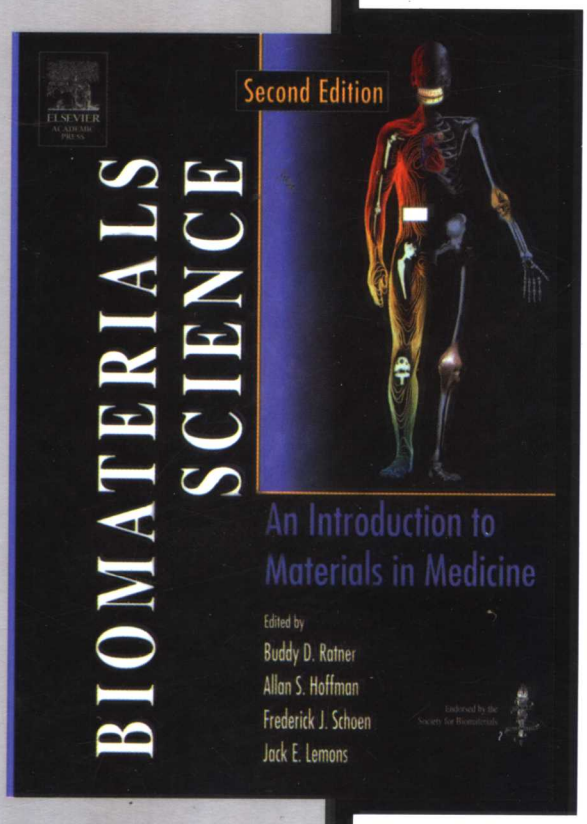

清华大学出版社

国外大学优秀教材——材料科学与工程系列（影印版）

生物材料科学
医用材料导论（第2版）

Biomaterials Science:
An Introduction to Materials in Medicine
(Second Edition)

Buddy D. Ratner
Allan S. Hoffman
Frederick J. Schoen
Jack E. Lemons

清华大学出版社
北京

Buddy D. Ratner, Allan S.Hoffman, Frederick J. Schoen, Jack E. Lemons
Biomaterials Science: An Introduction to Materials in Medicine, Second Edition
ISBN: 012582463-7, 978-0125824637

Authorized English language reprint edition published by the Proprietor.
ISBN: 981-259-803-0, 978-981-259-803-5

图书在版编目(CIP)数据

生物材料科学：医用材料导论：第2版 = Biomaterials Science: An Introduction to Materials in Medicine, 2th Edition /(美)拉特纳(Ratner, B. D.)等编著. —影印本. —北京：清华大学出版社，2006.12
（国外大学优秀教材. 材料科学与工程系列）
ISBN 7-302-14188-6

Ⅰ. 生… Ⅱ. 拉… Ⅲ. 生物医学工程－生物材料－高等学校－教材－英文 Ⅳ. R318.08

中国版本图书馆 CIP 数据核字（2006）第 141566 号

责任编辑：宋成斌
责任印制：何 芊

出版发行：清华大学出版社
http://www.tup.com.cn
c-service@tup.tsinghua.edu.cn
社 总 机：010-62770175
投稿咨询：010-62772015
地 址：北京清华大学学研大厦 A 座
邮 编：100084
邮购热线：010-62786544
客户服务：010-62776969

印 装 者：清华大学印刷厂
经 销：全国新华书店
开 本：214×278 **印 张**：54 **彩 插**：8
版 次：2006 年 12 月第 1 版 2006 年 12 月第 1 次印刷
印 数：1~3000
定 价：109.00 元

本书如存在文字不清、漏印、缺页、倒页、脱页等印装质量问题，请与清华大学出版社出版部联系调换。联系电话：010-62770177 转 3103 产品编号：013996-01

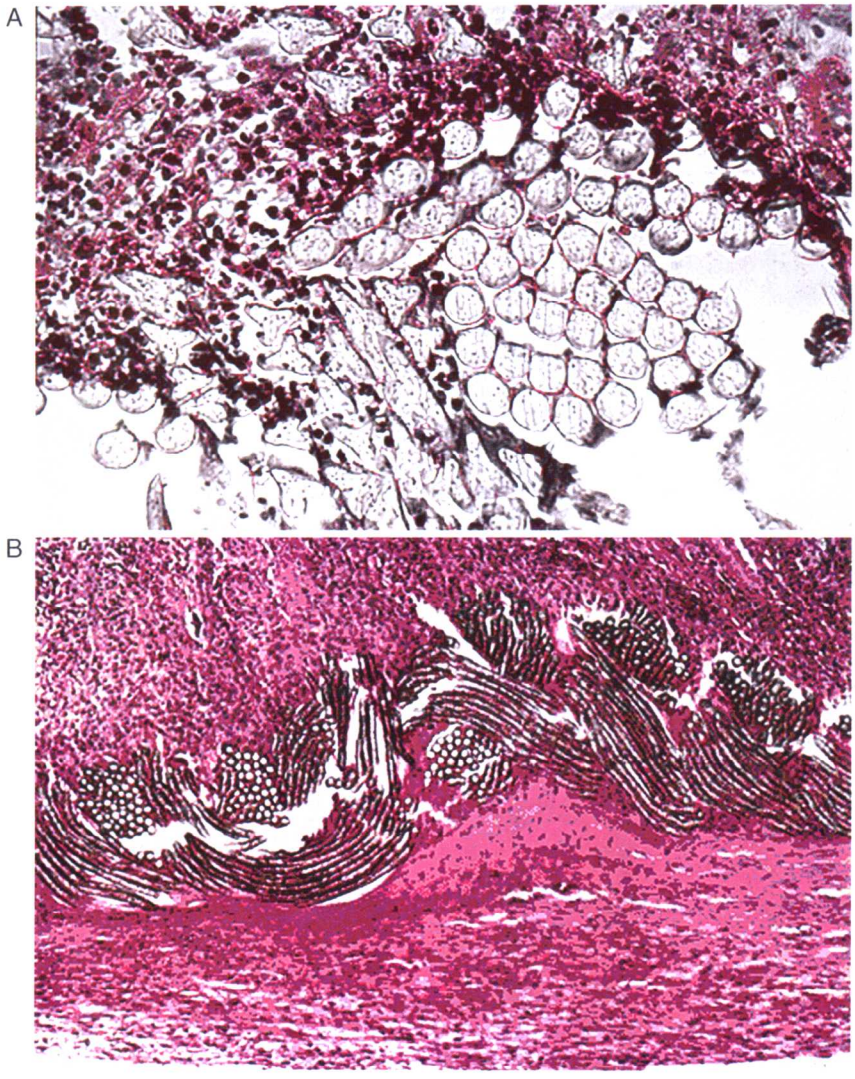

Chapter 2.4, Fig. 9 (A) Weft knit inflammatory response at 4 weeks (Golaski Microkit); (B) Warp knit inflammatory response at 3 days (Microvel).

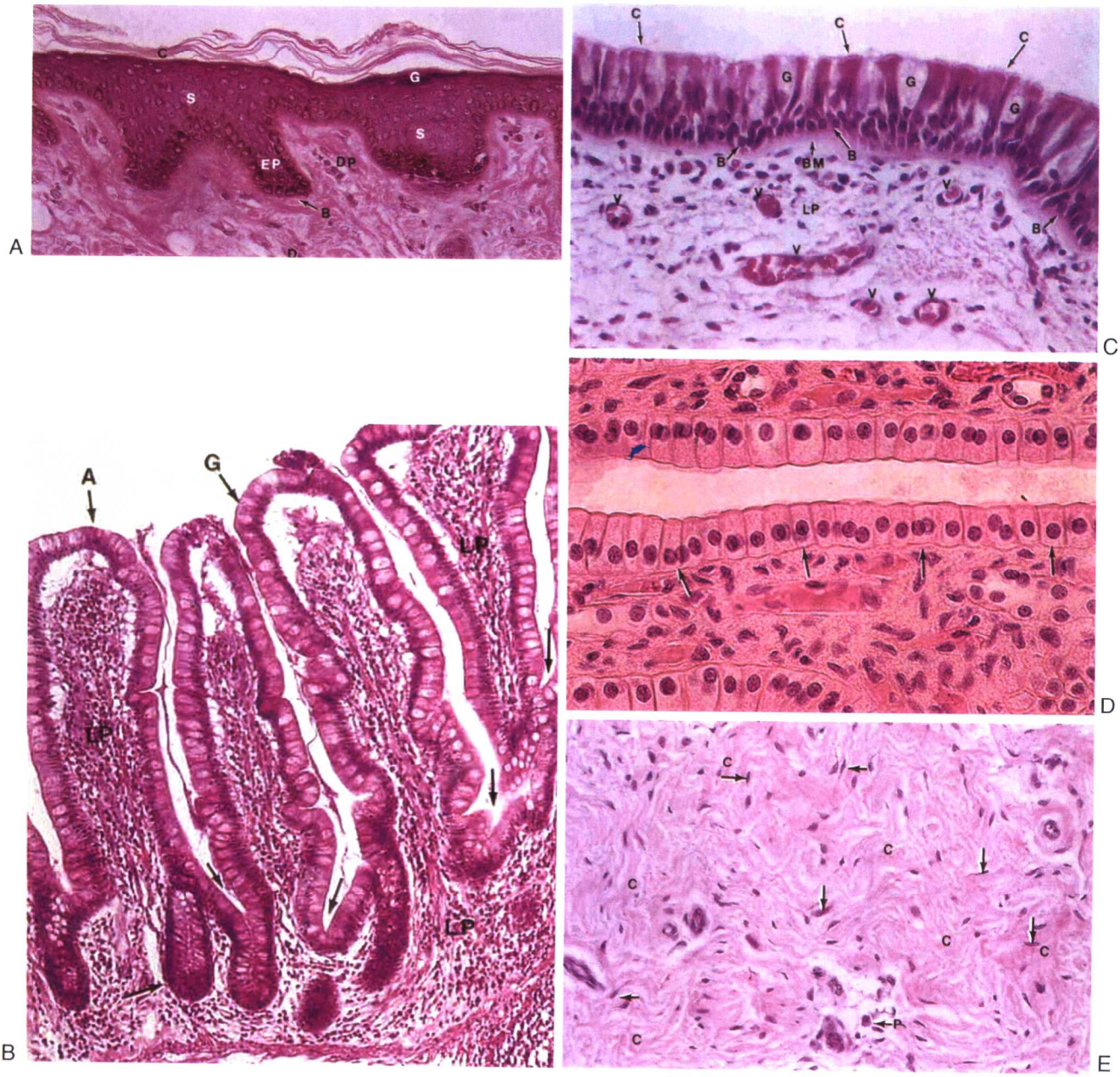

Chapter 3.4, Fig. 5 Photomicrographs of basic tissues, emphasizing key structural features. (A–D) Epithelium; (E, F) connective tissue; (G) muscle; and (H) nervous tissue. (A) Skin. Note the thin stratum corneum (c) and stratum granulosum (g). Also shown are the stratum spinosum (*s*), stratum basale (b), epidermal pegs (ep), dermal papilla (dp), and dermis (d). (B) Trachea, showing goblet cells (g), ciliated columnar cells (*c*), and basal cells (*B*). Note the thick basement membrane (bm) and numerous blood vessels (v) in the lamina propria (lp). (C) Mucosa of the small intestine (ileum). Note the goblet (g) and columnar absorbing (a) cells, the lamina propria (lp), muscularis mucosae (mm), and crypts (arrows). (D) Epithelium of a kidney collecting duct resting on a thin basement membrane (arrows). (E) Dense irregular connective tissue. Note the wavy unorientated collagen bundles (c) and fibroblasts (arrows). p, plasma cells. (F) Cancellous bone clearly illustrating the morphologic difference between inactive bone lining (endosteal, osteoprogenitor) cells (bl) and active osteoblasts (ob). The clear area between the osteoblasts and calcified bone represents unmineralized matrix or osteoid. cl, cement lines; o, osteocycles. H) Small nerve fascicles (n) with perineurium (p) separating it from two other fascicles (n). (A–F and H reproduced by permission from Berman, I., 1993. *Color Atlas of Basic Histology.* Appleton and Lange, 1993. G reproduced by permission from Schoen F. J., The heart. in *Robbins Pathologic Basis of Disease*, 7th ed., R. S. Cotran, V. Kumar and T. Collins, eds. Saunders, Philadelphia, in press.)

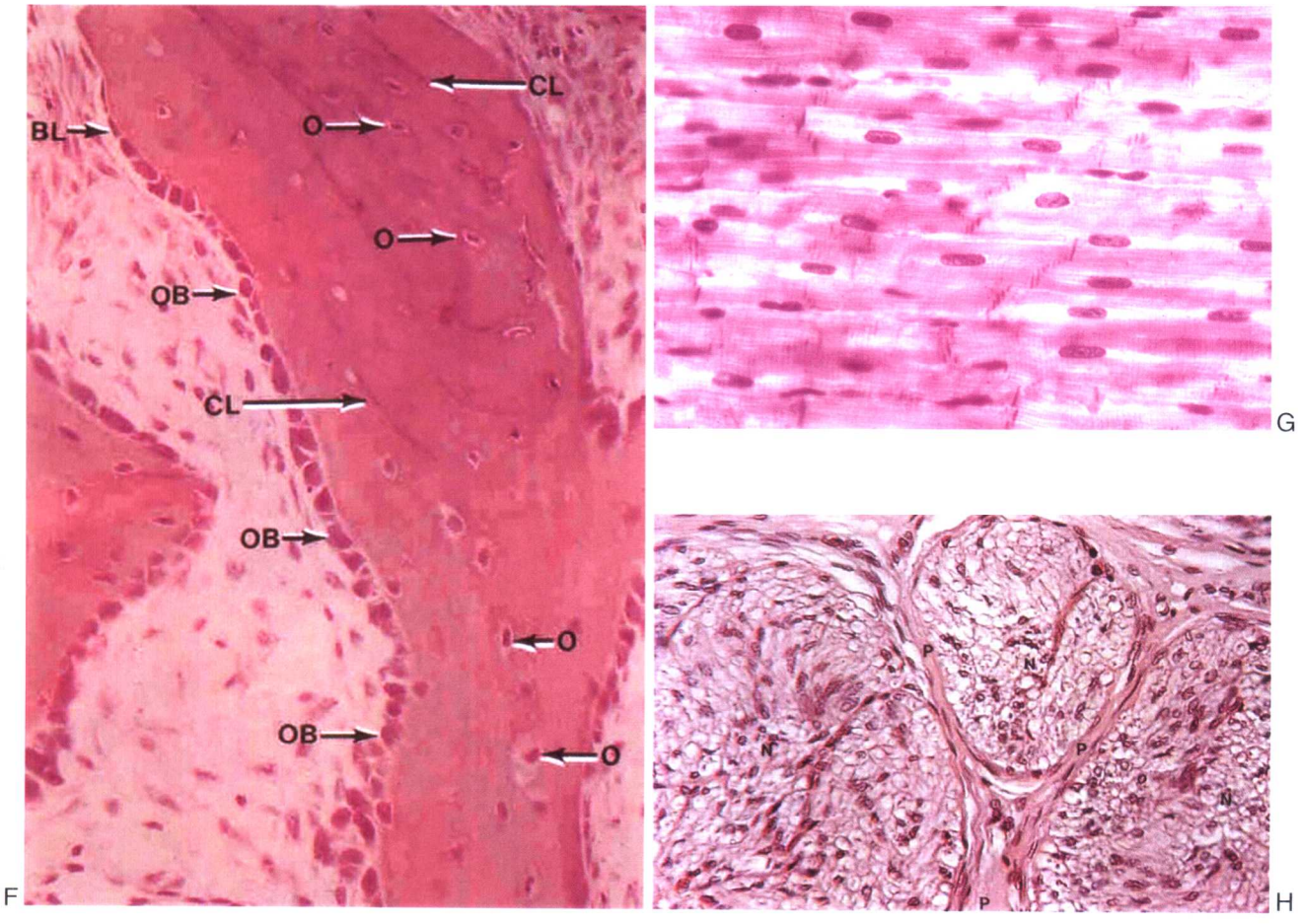

Chapter 3.4, Fig. 5—continued

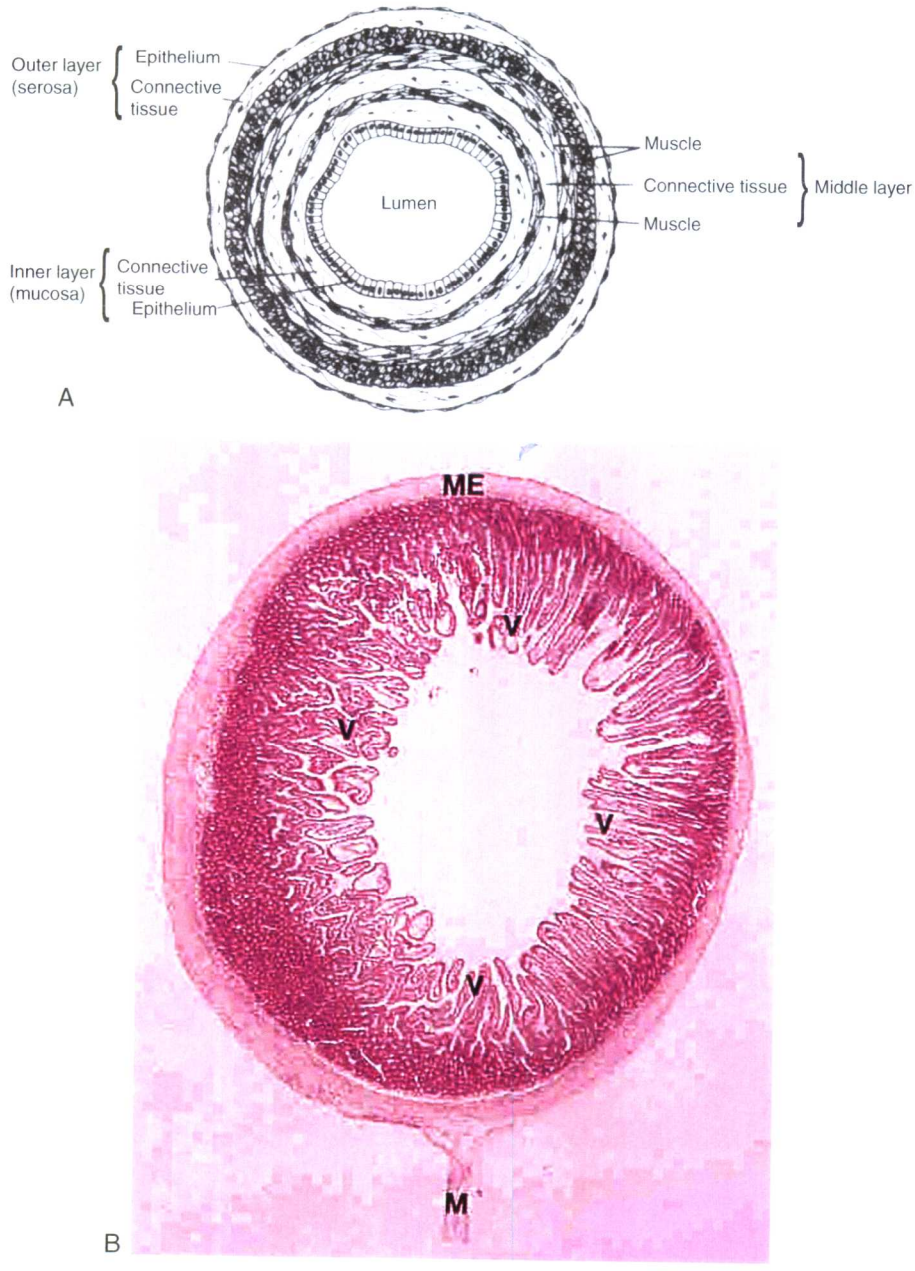

Chapter 3.4, Fig. 7 (A) Organization of tissue layers in the digestive tract (e.g., stomach or intestines). (B) Photomicrograph of the dog jejunum illustrating villi (v), the muscularis external (me), and mesentery (m). In this organ the epithelium is organized into folds (the villi) in order to increase the surface area for absorption. (A, Reproduced by permission from Borysenko, M., and Beringer, T., *Functional Histology*, 3rd ed. Copyright 1989 Little, Brown, and Co. B, Reproduced by permission from Berman, I., 1993. *Color Atlas of Basic Histology*, Appleton and Lange.)

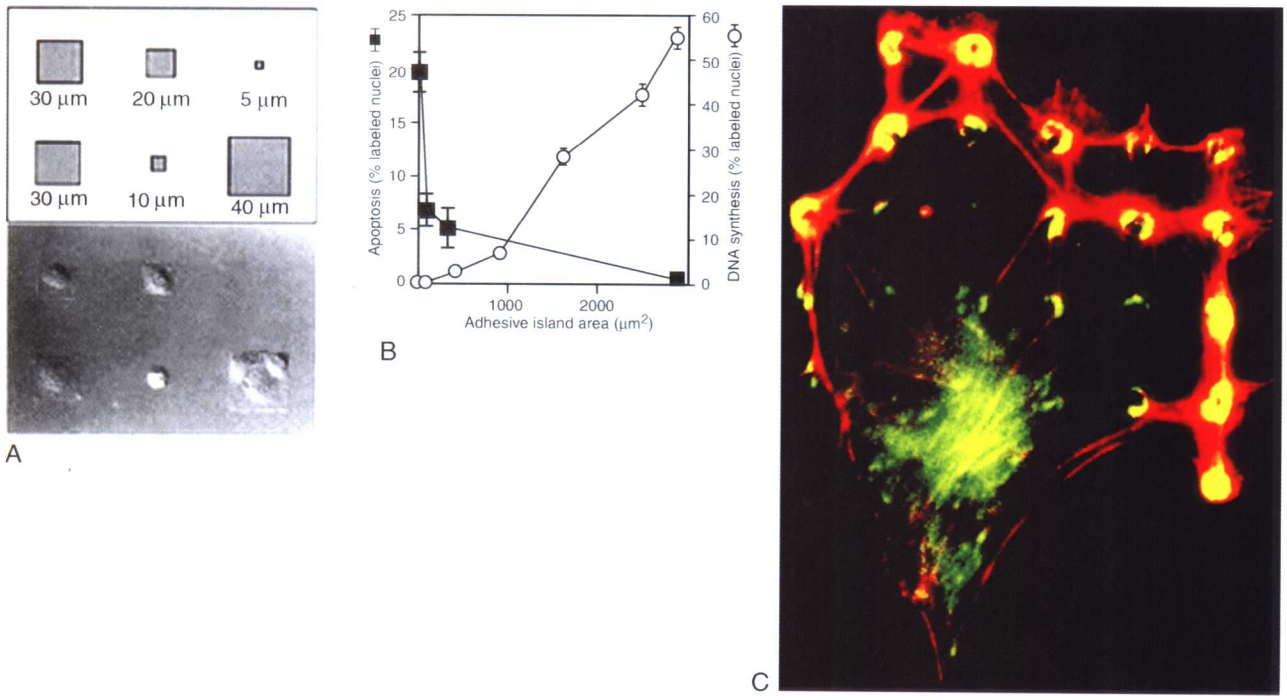

Chapter 3.4, Fig. 13 Effect of spreading on cell growth and apoptosis. (A) Schematic diagram showing the initial pattern design containing different-sized square adhesive islands and Nomarski views of the final shapes of bovine adrenal capillary endothelial cells adherent to the fabricated substrate. Distances indicate lengths of the squares' sides. (B) Apoptotic index (percentage of cells exhibiting positive TUNEL staining) and DNA synthesis index (percentage of nuclei labeled with 5-bromodeoxyuridine) after 24 hours, plotted as a function of the projected cell area. Data were obtained only from islands that contained single adherent cells; similar results were obtained with circular or square islands and with human or bovine endothelial cells. (C) Fluorescence micrograph of an endothelial cell spread over a substrate containing a regular array of small (5-μm-diameter) circular ECM islands separated by nonadhesive regions created with a microcontact printing technique. Yellow rings and crescents indicate colocalization of vinculin (green) and F-actin (red) within focal adhesions that form only on the regulatory spaced circular ECM islands. (A, B, Reproduced by permission from Chen, C. S., *et al.*, 1997. Geometric control of cell life and death. *Science* **276:** 1425. C, Reproduced by permission from Ingber, D. E., 2003. Mechanosensation through integrins: Cells act locally but think globally. *Proc. Natl. Acad. Sci. USA* **100:** 1472.)

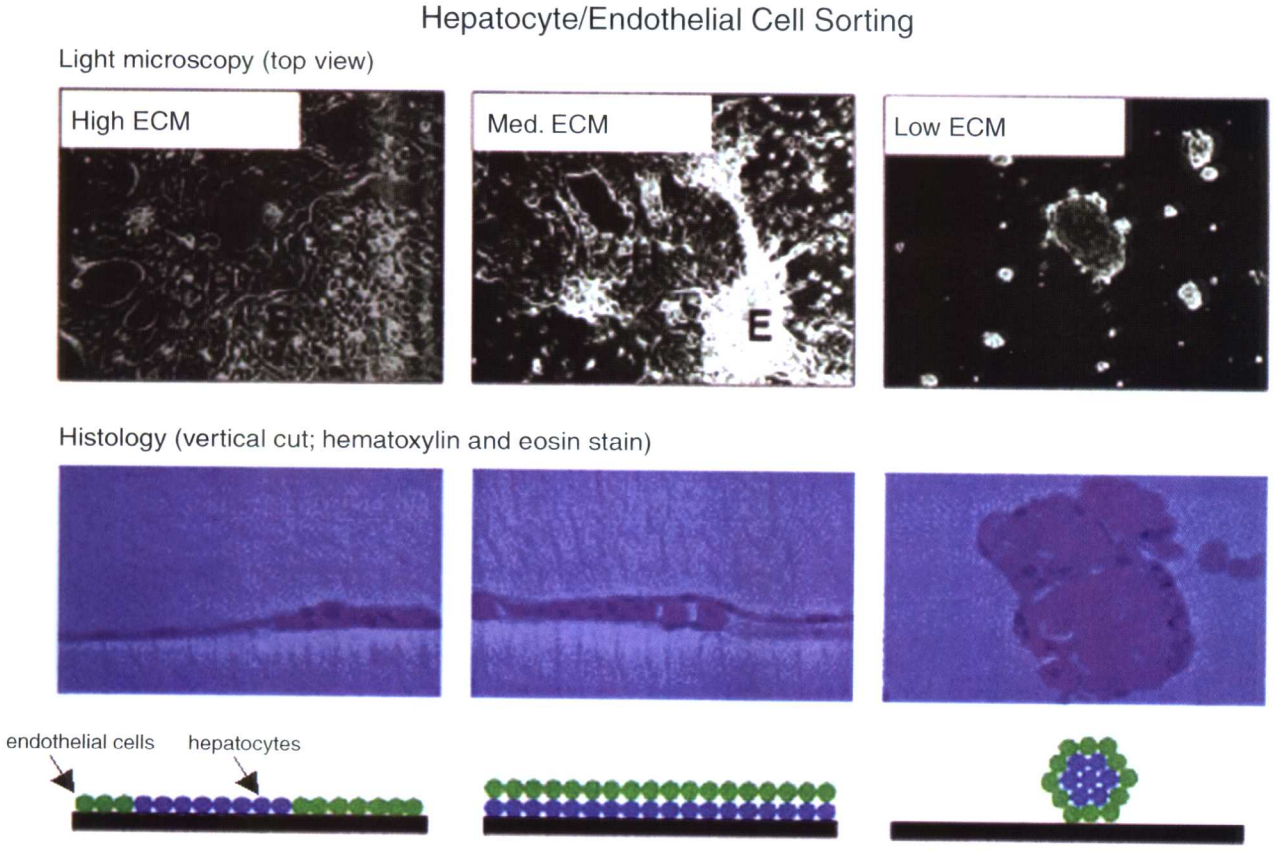

Chapter 3.4, Fig. 14 Different levels of type 1 collagen coating on a culture dish result in different organization of endothelial cells and hepatocytes. High collagen levels cause both cell types to spread across the substratum (left). On intermediate collagen levels, endothelial cells form a layer on the substratum whereas hepatocytes form a layer on top of the endothelial cells (center). Low levels of collagen result in an inner layer of hepatocyte aggregate surrounded by endothelial cells (right). (Reproduced by permission from Lauffenburger, D. A., *et al.*, 2001. Who's got pull around here? Cell organization in development and tissue engineering. *Proc. Natl. Acad. Sci. USA* 98: 4282.)

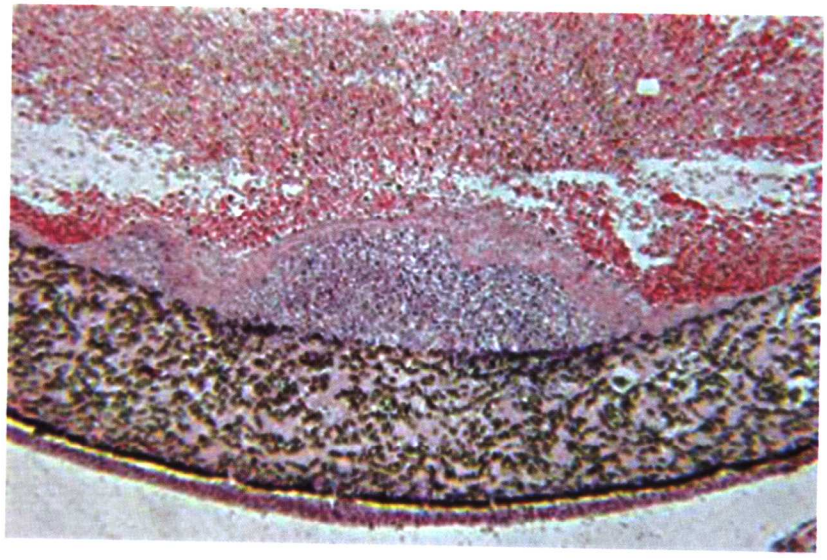

Chapter 4.2, Fig. 2 Acute inflammation, secondary to infection, of an ePTFE vascular graft. A focal zone of polymorphonuclear leukocytes is present at the lumenal surface of the vascular graft, surrounded by a fibrin cap, on the blood-contacting surface of the ePTFE vascular graft. Hematoxylin and eosin stain. Original magnification 4×.

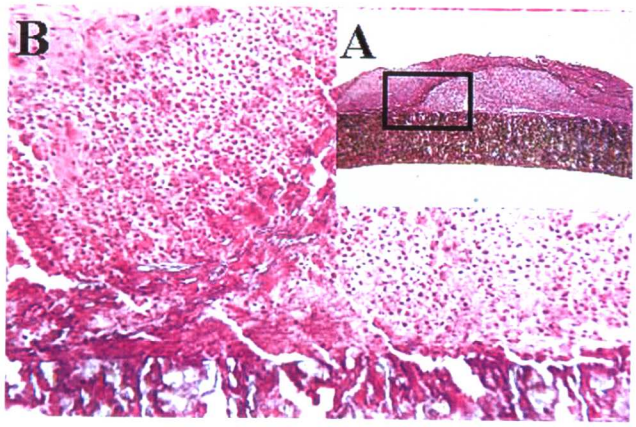

Chapter 4.2, Fig. 3 Chronic inflammation, secondary to infection, of an ePTFE arteriovenous shunt for renal dialysis. (A) Low-magnification view of a focal zone of chronic inflammation. (B) High-magnification view of the outer surface with the presence of monocytes and lymphocytes at an area where the outer PTFE wrap had peeled away from the vascular graft. Hematoxylin and eosin stain. Original magnification (A) 4×, (B) 20×.

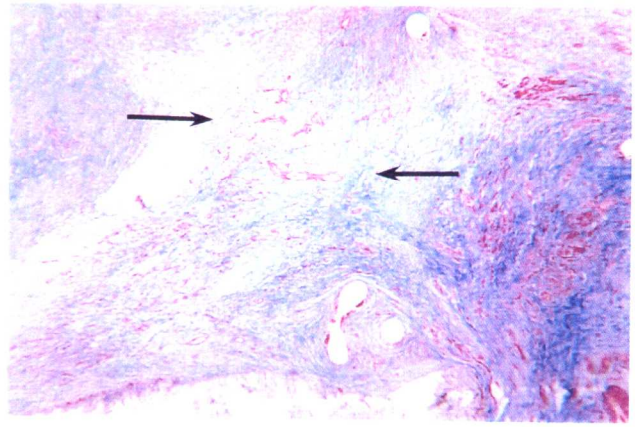

Chapter 4.2, Fig. 4 Granulation tissue in the anastomotic hyperplasia at the anastomosis of an ePTFE vascular graft. Capillary development (red slits) and fibroblast infiltration with collagen deposition (blue) from the artery form the granulation tissue (arrows). Masson's Trichrome stain. Original magnification 4×.

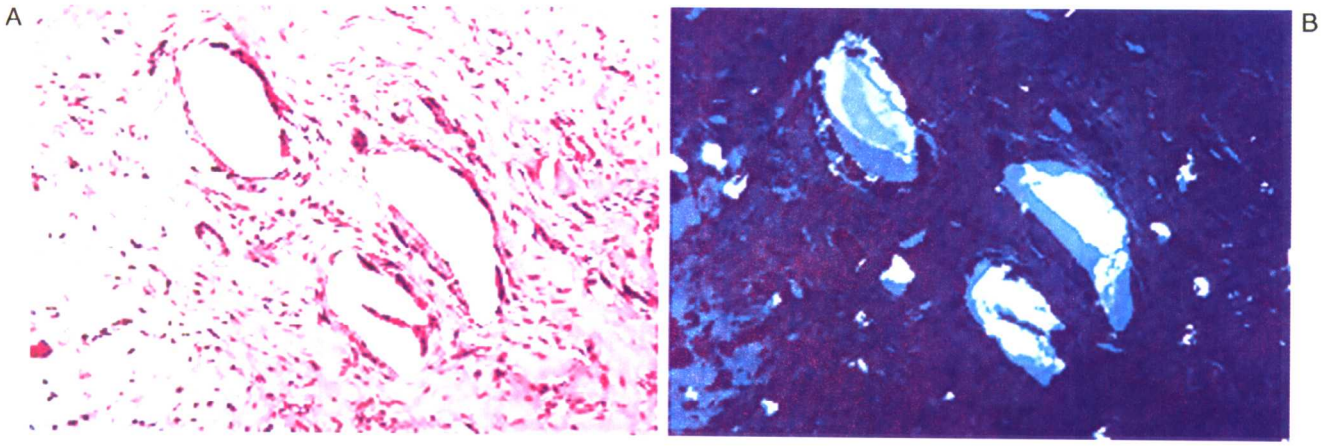

Chapter 4.2, Fig. 6 (A) Focal foreign-body reaction to polyethylene wear particulate from a total knee prosthesis. Macrophages and foreign-body giant cells are identified within the tissue and lining the apparent void spaces indicative of polyethylene particulate. Hematoxylin and eosin stain. Original magnification 20×. (B) Partial polarized light view. Polyethylene particulate is identified within the void spaces commonly seen under normal light microscopy. Hematoxylin and eosin stain. Original magnification 20×.

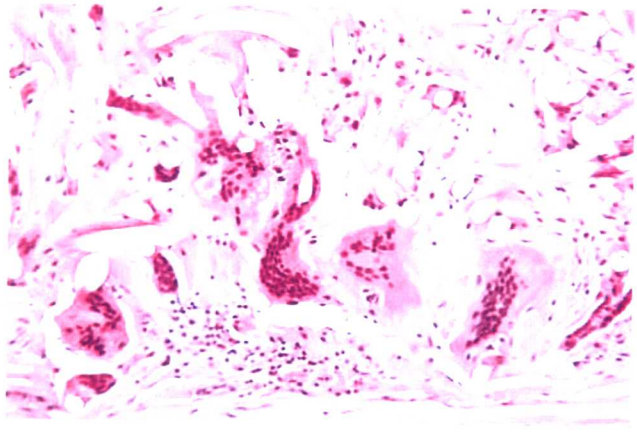

Chapter 4.2, Fig. 7 Foreign-body reaction with multinucleated foreign body giant cells and macrophages at the periadventitial (outer) surface of a Dacron vascular graft. Fibers from the Dacron vascular graft are identified as clear oval voids. Hematoxylin and eosin stain. Original magnification 20×.

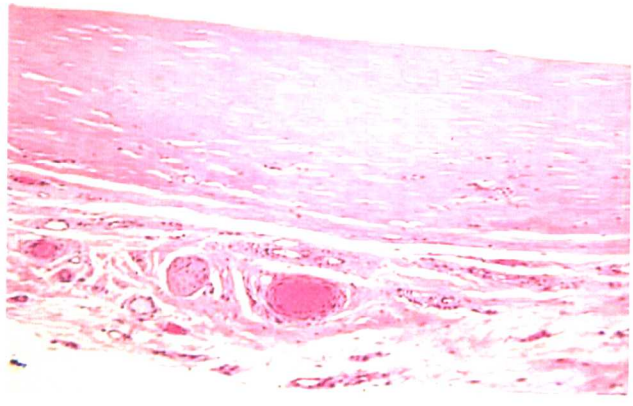

Chapter 4.2, Fig. 9 Fibrous capsule composed of dense, compacted collagen. This fibrous capsule had formed around a Mediport catheter reservoir. Loose connective tissue with small arteries, veins, and a nerve is identified below the acellular fibrous capsule.

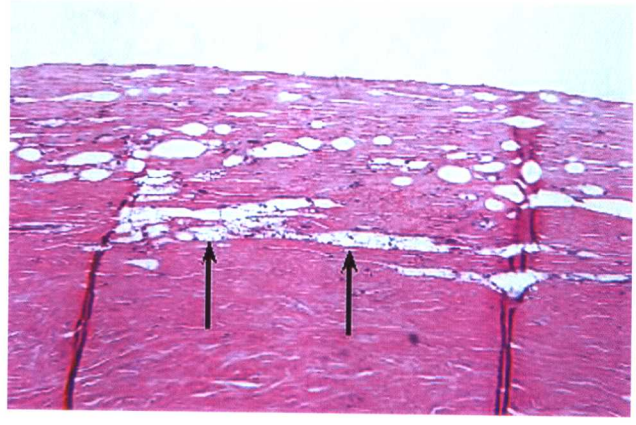

Chapter 4.2, Fig. 10 Fibrous capsule with a focal foreign-body reaction to silicone gel from a silicone gel–filled silicone-rubber breast prosthesis. The breast prosthesis–tissue interface is at the top of the photomicrograph. Oval void spaces lined by macrophages and a few giant cells are identified and a focal area of foamy macrophages (arrows) indicating macrophage phagocytosis of silicone gel is identified. Hematoxylin and eosin stain. Original magnification 10×.

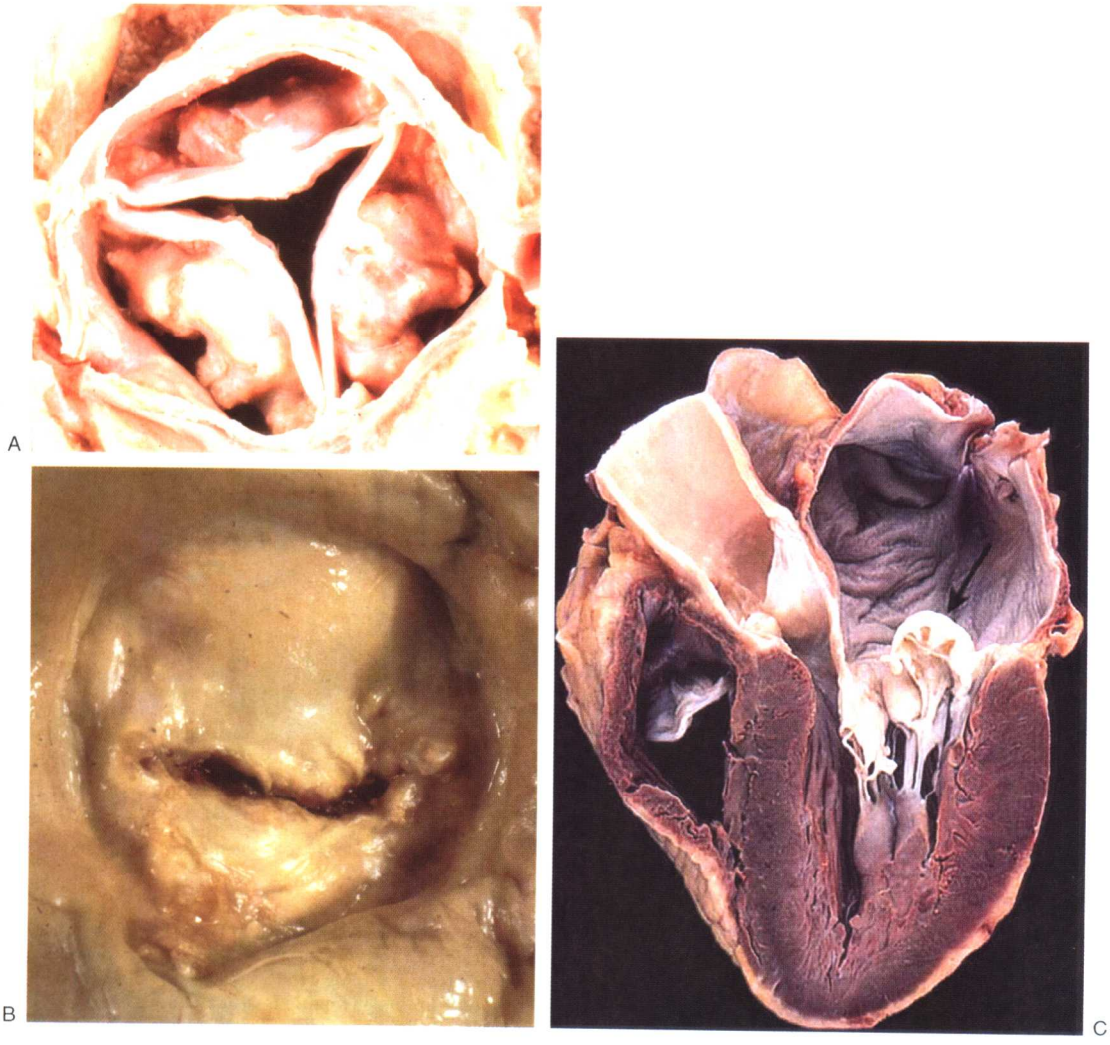

Chapter 7.3, Fig. 2 (A) Severe degenerative calcification of a previously anatomically normal tricuspid aortic valve, the predominant cause of aortic stenosis. (B) Chronic rheumatic heart disease, manifest as mitral stenosis, viewed from the left atrium. (C) Myxomatous degeneration of the mitral valve, demonstrating hooding with prolapse of the posterior mitral leaflet into the left atrium (*arrow*). A, B: Reproduced by permission from Schoen, F. J., and Edwards, W. D. (2001). Valvular heart disease: General priciples and stenosis. in *Cardiovascular Pathology*, 3rd ed. Silver, M. D., Gotlieb, A. I., and Schoen, F. J., eds. Churchill Livingstone, New York. C: Reproduced by permission from Schoen, F. J. (1999). The heart. in *Robbins Pathologic Basis of Disease*, 6th ed., R. S. Cotran, V. Kumar, T. Collins, eds. W.B. Saunders, Philadelphia.

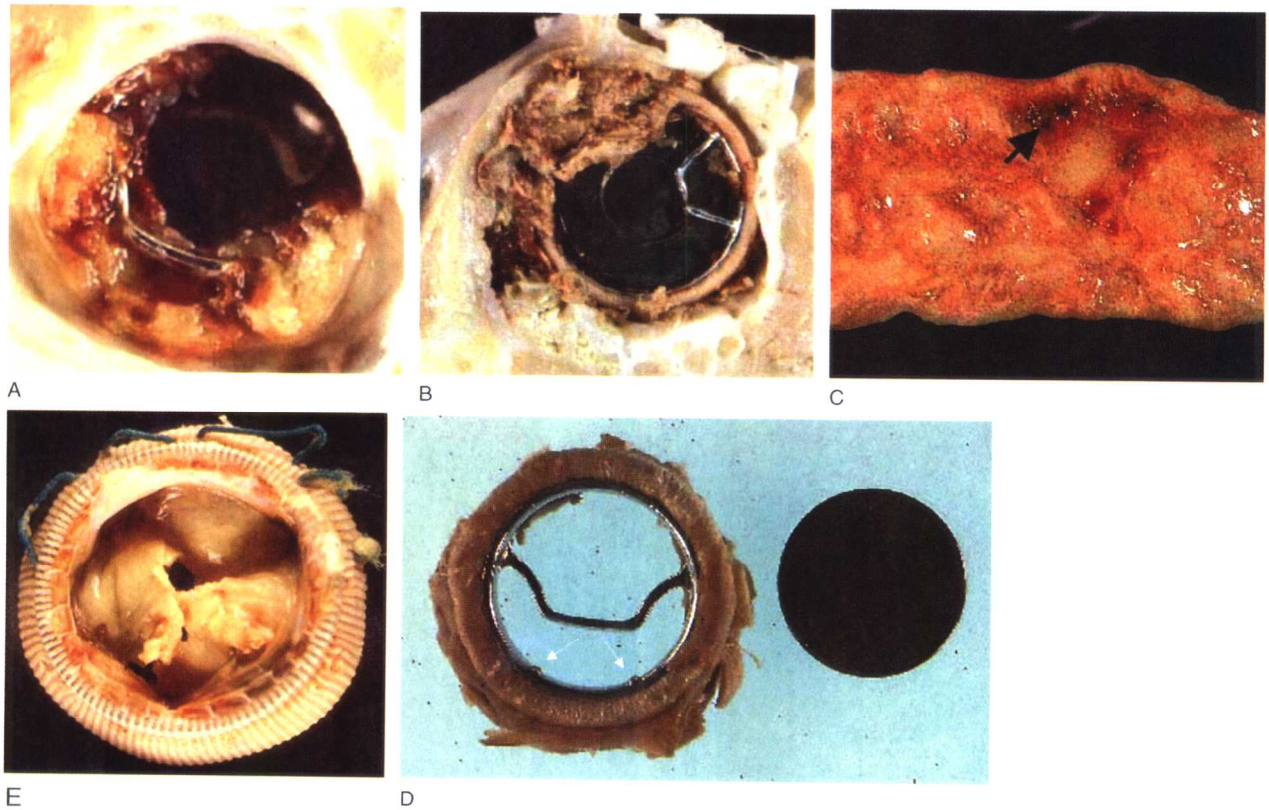

Chapter 7.3, Fig. 6 Prosthetic valve complications. (A) Thrombosis on a Bjork–Shiley tilting disk aortic valve prosthesis, localized to outflow strut near minor orifice, a point of flow stasis. (B) Thromboembolic infarct of the small bowel (arrow) secondary to embolus from valve prosthesis. (C) Prosthetic valve endocarditis with large ring abscess, viewed from the ventricular aspect of an aortic Bjork–Shiley tilting disk aortic valve. (D) Strut fracture of Bjork–Shiley valve, showing valve housing with single remaining strut and adjacent disk. (E) Structural valve dysfunction (manifest as calcific degeneration with tear) of porcine valve. B: Reproduced by permission from Schoen, F. J. (2001). Pathology of heart valve substitution with mechanical and tissue prostheses. in *Cardiovascular Pathology*, 3rd ed. M. D. Silver, A. I. Gotlieb, and F. J. Schoen, eds. Churchill Livingstone, New York. C: Reproduced by permission from Schoen, F. J. (1987). Cardiac valve prostheses: pathological and bioengineering considerations. *J. Card. Surg.* **2**: 65. A and D: Reproduced by permission from Schoen, F. J., Levy, R. J., and Piehler, H. R. (1992). Pathological considerations in replacement cardiac valves. *Cardiovasc. Pathol.* **1**: 29.

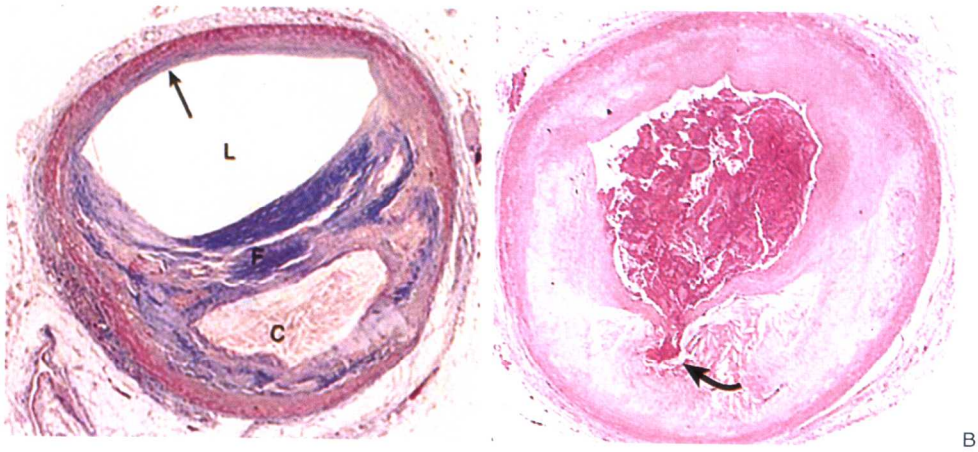

Chapter 7.3, Fig. 7 Atherosclerotic plaque in the coronary artery. (A) Overall architecture demonstrating a fibrous cap (F) and a central lipid core (C) with typical cholesterol clefts. The lumen (L) has been moderately narrowed. Note the plaque-free segment of the wall (*arrow*). (B) Coronary thrombosis superimposed on an atherosclerotic plaque with focal disruption of the fibrous cap (*arrow*), triggering fatal myocardial infarction. A: Reproduced by permission from Schoen, F. J., and Cotran, R. S. (1999). Blood vessels. in *Robbins Pathologic Basis of Disease*, 6th ed., R. S. Cotran, V. Kumar, and T. Collins, eds. W.B. Saunders, Philadelphia. B: Reproduced by permission from Schoen, F. J. (1989). *Interventional and Surgical Cardiovascular Pathology: Clinical Correlations and Basic Principles*. W.B. Saunders, Philadelphia.

Chapter 7.3, Fig. 10 Stent grafts. (A) Configuration of device showing composite metal and fabric portions. (B) Low-power photomicrograph of well-healed experimental device explanted from a dog aorta. The lumen is widely patent and the fabric and metal components are visible. (C) High-power photomicrograph of stent graft interaction with the vascular wall, demonstrating mild intimal thickening. B and C: courtesy Jagdish Butany, MD, University of Toronto.